

Constrained Sparse Galerkin Regression

J.-Ch. Loiseau¹ and S. L. Brunton²

¹Laboratoire DynFluid, Arts et Métiers ParisTech, 75013 Paris, France

²Department of Mechanical Engineering, University of Washington, Seattle, WA 98195, USA

Abstract

In this work, we demonstrate the use of sparse regression techniques from machine learning to identify nonlinear low-order models of a fluid system purely from measurement data. In particular, we extend the sparse identification of nonlinear dynamics (SINDy) algorithm to enforce physical constraints in the regression, leading to energy conservation. The resulting models are closely related to Galerkin projection models, but the present method does not require the use of a full-order or high-fidelity Navier-Stokes solver to project onto basis modes. Instead, the most parsimonious nonlinear model is determined that is consistent with observed measurement data and satisfies necessary constraints. The constrained Galerkin regression algorithm is implemented on the fluid flow past a circular cylinder, demonstrating the ability to accurately construct models from data.

1 Introduction

Identifying accurate and efficient reduced-order models is a central challenge in computational fluid dynamics and closed-loop flow control (Brunton and Noack, 2015; Fabbiane et al., 2014; Sipp and Schmid, 2016). Fluid flows are characterized by high-dimensional, nonlinear dynamics that give rise to rich structures. Despite this apparent complexity, the dynamics often evolve on a low-dimensional attractor defined by a few dominant coherent structures that contain significant energy or are useful for control (Holmes et al., 2012). This property allows one to construct or identify low-dimensional reduced-order models that reproduce qualitatively and quantitatively the dynamics of the full system.

Many traditional model reduction techniques are analytical. They rely on knowledge of the full high-fidelity Navier-Stokes equations to project onto an orthogonal basis, resulting in a dynamical system in terms of the coefficients of the basis modes. These modes may come from a classical expansion, such as Fourier modes, or they may be data-driven, as in the proper orthogonal decomposition (POD) (Berkooz et al., 1993; Sirovich, 1987). In the latter case, the model-reduction may be considered a hybrid approach, mixing knowledge of the physics with empirical modes obtained from measurement data. In the framework of fluid dynamics, Noack et al. (2003) have shown that such reduced-order models obtained from a Galerkin projection can reproduce the non-linear dynamics of the von Kàrmàn vortex shedding past a two-dimensional cylinder, provided that the projection basis includes a *shift mode* quantifying the distortion between the linearly unstable base

flow and marginally stable mean flow. Recently, Semaan et al. (2016) have extended the reduced-order modeling strategy of Noack et al. (2003) to include the effect of control actuation for the flow around a high-lift configuration airfoil.

In contrast, data-driven approaches are becoming increasingly important. System identification encompasses a large body of work identifying dynamical systems models from measurement data, and recent advances in machine learning are greatly expanding the ability to extract governing dynamics from data. In particular, advanced regression methods from statistics, such as genetic programming or sparse regression, are driving new algorithms that identify nonlinear dynamics from measurements of complex systems. Bongard and Lipson (2007) and Schmidt and Lipson (2009) introduced nonlinear system identification based on genetic programming, which has been used in numerous practical applications in aerospace engineering, the petroleum industry, and in finance. These algorithms have since been incorporated into the software Eureka by Nutonian[®]. More recently, Brunton et al. (2016) have proposed a system identification approach based on sparse regression known as the sparse identification of nonlinear dynamics (SINDy). Following the principle of Ockham’s razor, the SINDy algorithm rests on the assumption that there are only a few important terms that govern the dynamics of a given system, so that the equations are sparse in the space of possible functions. Sparse regression is then used to determine the fewest terms in a dynamical system required to accurately represent the data. The resulting models are parsimonious, balancing model complexity with descriptive power while avoiding overfitting. Moreover, sparse models may be more readily interpretable as the structure can be amenable to normal form or bifurcation analysis.

Though they are relatively simple to implement, a major drawback of regression-based methods is the loss of underlying physical constraints or symmetries, which may be included in the physics-based Galerkin projection methods described previously (Balajewicz et al., 2013). A notable exception is the physics-constrained multi-level quadratic regression used to identify models in climate and turbulence (Majda and Harlim, 2012). In this work, we extend the SINDy algorithm (Brunton et al., 2016), which identifies nonlinear dynamical systems through sparse regression, generalizing it to include physical constraints such as conservation of energy or enforce symmetries in the identified equations. The resulting algorithm relies on the use of constrained least squares (Golub and Van Loan, 2012) to incorporate additional constraints in the SINDy algorithm for the sparse identification of the underlying low-dimensional dynamical system. The ability of the present system identification technique, hereafter named *constrained sparse Galerkin regression*, is demonstrated on the emblematic two-dimensional cylinder flow.

2 Constrained sparse identification

Let us consider a dynamical system of the form

$$\dot{\mathbf{x}} = \mathbf{f}(\mathbf{x}) \tag{1}$$

where $\mathbf{x}(t)$ is the state vector of the system. For many systems, the function \mathbf{f} is sparse in the space of possible functions, *i.e.* it only contains a few non-zero terms. Let us assume for simplicity, and without loss of generality, that the dynamical system (1) has only three degrees of freedom such that $\mathbf{x} = [x, y, z]^T$. To identify the function \mathbf{f} from data, the time history of the state $\mathbf{x}(t)$ and its derivative $\dot{\mathbf{x}}(t)$ are collected at several times t_1, t_2, \dots, t_m and arranged into two column vectors:

$$\mathbf{X} = [x(t_1) \ \cdots \ x(t_m) \ y(t_1) \ \cdots \ y(t_m) \ z(t_1) \ \cdots \ z(t_m)]^T \quad (2a)$$

$$\dot{\mathbf{X}} = [\dot{x}(t_1) \ \cdots \ \dot{x}(t_m) \ \dot{y}(t_1) \ \cdots \ \dot{y}(t_m) \ \dot{z}(t_1) \ \cdots \ \dot{z}(t_m)]^T. \quad (2b)$$

Next, a library $\Theta(\mathbf{x})$ is constructed from the data, where each column is a candidate linear or nonlinear function of x , y and z for the right-hand side of (1), evaluated using the m data points in (2a). One can then write

$$\dot{\mathbf{X}} = \begin{bmatrix} \Theta(\mathbf{x}) & 0 & 0 \\ 0 & \Theta(\mathbf{x}) & 0 \\ 0 & 0 & \Theta(\mathbf{x}) \end{bmatrix} \begin{bmatrix} \xi_x \\ \xi_y \\ \xi_z \end{bmatrix} \quad (3)$$

where $\xi = [\xi_x, \xi_y, \xi_z]^T$ is a vector containing the coefficients of each candidate function stored in the columns of $\Theta(\mathbf{x})$ for the x , y and z equations. Given that \mathbf{f} is sparse in the space of possible functions, ξ can be identified using sparse regression techniques. Such an approach to system identification is known as Sparse Identification of Nonlinear Dynamics (Brunton et al., 2016), or simply SINDy. Note that the variable stacking in (2) and (3) differs slightly from the original SINDy algorithm, in that time-series of variables are stacked vertically into a single column vector, rather than as individual columns in a matrix, making it easier to add constraints on the coefficients in ξ .

In the present work, we build upon SINDy and include additional constraints on the entries of ξ beyond the constraint of sparsity. The regression problem then reads

$$\begin{aligned} \min_{\xi} \|\dot{\mathbf{X}} - \mathbf{L}\xi\|_2^2 \\ \text{such that } \mathbf{C}\xi = \mathbf{d} \end{aligned} \quad (4)$$

where \mathbf{L} is the block-diagonal matrix in (3) and $\|\cdot\|_2$ is the Euclidean norm. The matrix \mathbf{C} and vector \mathbf{d} impose the user-provided constraints on the regression coefficients in ξ . As before, sparsity is promoted by adding an l_1 penalization to the minimization problem (4), or by using the sequential thresholded least-squares algorithm as in Brunton et al. (2016). In the present work, the latter option is used. After an initial constrained least-squares regression, the thresholding is then performed as follows: if $|\xi_i|$ is smaller than λ (the sparsity knob) times the mean of the absolute value of the non-zero entries of ξ , then an additional row is added to the constraint matrix \mathbf{C} to enforce $\xi_i = 0$. Two or three iterations of this small variation of the sequential thresholded least-squares algorithm are usually sufficient to ensure convergence of the constrained minimization procedure. Though it has been assumed for the sake of simplicity that the library $\Theta(\mathbf{x})$ and sparsity knob λ are the same for each equation, these assumptions can easily be relaxed and require only minor modifications in the algorithm's numerical implementation.

Finally, let us discuss the influence of the sparsity knob λ . If λ is too small, no terms are eliminated. On the other hand, if λ is too large, the identified model may have too few terms. To evaluate *a priori* the predictive capabilities of the identified model, it is convenient to analyze the number of non-zero coefficients and the r^2 score (Draper and Smith, 2014) as a function of the sparsity knob λ . This is depicted in figure 1 for one of the models identified in §3.3, and as the sparsity knob λ is increased from 10^{-5} to 0.1, the number of non-zero coefficients identified in the model decreases from 21 for $\lambda = 10^{-5}$ to 11 for $\lambda = 0.1$ without altering the r^2 score of the

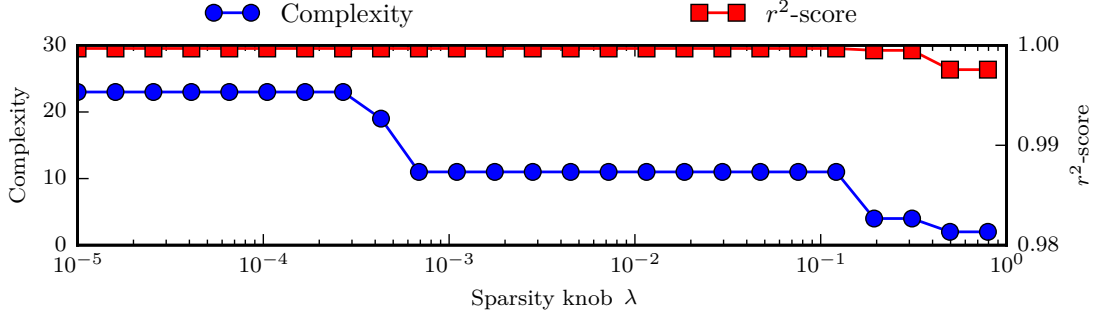


Figure 1: Example of the evolution of the identified model’s complexity (number of non-zero coefficients) and r^2 -score as a function of the sparsity knob λ used in the SINDy algorithm.

model. Finally, as the sparsity knob is increased from $\lambda = 0.1$ to $\lambda = 0.2$, the number of non-zero coefficients suddenly drops to only 6, hindering in the process the r^2 score of the identified model. This sudden drop indicates that some small yet crucial coefficients have been removed from the identified model as a result of the overly aggressive sparsity constraint. Similar trends have been observed for all the models presented herein. In the rest of this work, the different models have been identified using a sparsity knob varying between $\lambda = 0.01$ and $\lambda = 0.05$.

Notes on the numerical implementation: The constrained sparse regression algorithm is implemented in Python. It uses the CVXOPT library (Andersen et al., 2013) to solve the constrained least-squares problem. Moreover, every time an additional sparsity constraint is added as a new row to the matrix \mathbf{C} , a QR rank-revealing decomposition of \mathbf{C} is performed using SciPy (Jones et al., 2001) to ensure it has full rank (*i.e.* no linearly dependant constraints). Finally, if the same library $\Theta(\mathbf{x})$ is used for each equation in (3), only one instance of $\Theta(\mathbf{x})$ needs to be stored in memory. In case of different libraries for each equation, the matrix \mathbf{L} then relies on a sparse matrix representation to reduce its memory footprint when large datasets are considered. The algorithm, the datasets used in the present work, and an illustrative IPython notebook on the Lorenz system are freely available online (<https://github.com/loiseaujc/SINDy>).

3 Results

3.1 Two-dimensional cylinder flow

The flow configuration considered in the present work is the two-dimensional incompressible viscous flow past a circular cylinder at $Re = 100$. This Reynolds number, based on the free-stream velocity U_∞ , the cylinder diameter D and the kinematic viscosity ν , is well above the onset of vortex shedding (Schumm et al., 1994; Zebib, 1987) and below the onset of three-dimensional instabilities (Barkley and Henderson, 1996; Zhang et al., 1995). In the fluid dynamics community, a large body of literature exists in which this particular setup has been chosen to illustrate modal decomposition (Bagheri, 2013) and model identification techniques (Brunton et al., 2016; Noack et al., 2003; Sengupta et al., 2015). This setup is thus a particularly compelling test case to illustrate our model identification strategy, as well as to draw connections and quantify its performance against other well-established techniques.

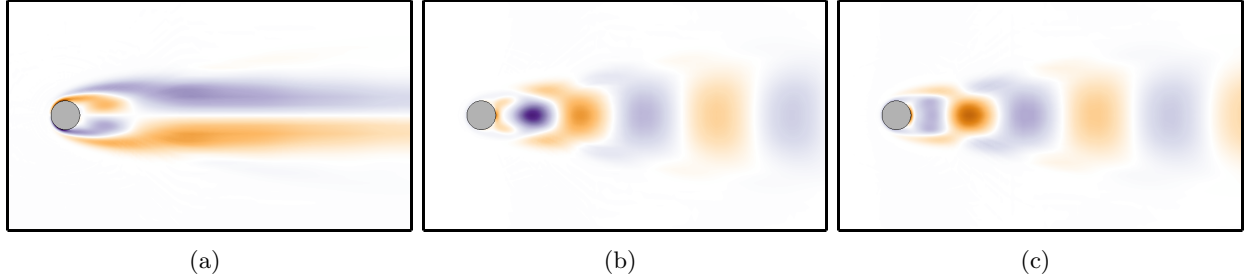


Figure 2: Vorticity fields of (a) the shift mode, (b) the first and (c) second POD modes of the cylinder flow at $Re = 100$.

The dynamics of the flow are governed by the incompressible Navier-Stokes equations. These are solved numerically using the Nek 5000 spectral element solver (Fischer et al., 2008). The computational domain extends from $x_1 = -20$ up to $x_1 = 60$ in the streamwise direction, and from $x_2 = -20$ up to $x_2 = 20$ in the spanwise direction. It is discretised using 2520 fifth-order spectral elements. Classic inflow-outflow conditions are imposed in the streamwise direction, while periodic boundary conditions are imposed in the spanwise direction. Finally, time integration is performed using the third-order accurate BDF3/EXT3 time-stepping scheme.

Given the linearly unstable base flow \mathbf{U}_b as initial condition, a direct numerical simulation has been run until a statistically steady-state has been achieved. The dynamics of the system on the final attractor are then equidistantly sampled using $M = 1000$ velocity field snapshots with a sampling frequency about 30 times larger than the vortex shedding frequency (Noack et al., 2015). The shift mode, denoted \mathbf{u}_Δ , is depicted in figure 2(a). This mode quantifies the distortion between the unstable base flow equilibrium and the mean flow. It has been shown to be crucially important for POD-based reduced-order modeling (Noack et al., 2003; Tadmor et al., 2010). The snapshot POD method of Sirovich (1987) has then been used to extract the two most energetic modes \mathbf{u}_1 and \mathbf{u}_2 , depicted in figures 2(b) and 2(c), respectively. Note that POD is performed using only a subset of the whole computational domain given by $-6 \leq x_1 \leq 15$ and $|x_2| \leq 3$, with x_1 and x_2 being the streamwise and spanwise coordinates. This observation window is similar to the computational domain used in the seminal work of Noack et al. (2003). A second DNS has then been performed, using $\mathbf{U}(\mathbf{x}, 0) = \mathbf{U}_b + 2\mathbf{u}_\Delta$ as the initial condition. The evolution in time of the POD coefficients is shown on figure 3(a), while a projection of the system's trajectory onto the $a_1 - a_\Delta$ plane is depicted on figure 3(b), where $a_1(t)$ is the amplitude of the POD mode \mathbf{u}_1 and $a_\Delta(t)$ the amplitude of the shift mode \mathbf{u}_Δ . As expected, the flow is first attracted toward the vicinity of the unstable fixed point \mathbf{U}_b ($\mathbf{x} = 0$ in the present visualisation) before being repelled. It eventually settles onto the limit cycle attractor, characterized by von Kàrmàn vortex shedding. These signals and their time derivatives (not shown) form the training dataset used to identify the models in §3.3.

3.2 Deriving the constraints

The Navier-Stokes equations governing the dynamics of the perturbation \mathbf{u} evolving on top of the base flow \mathbf{U}_b are given by

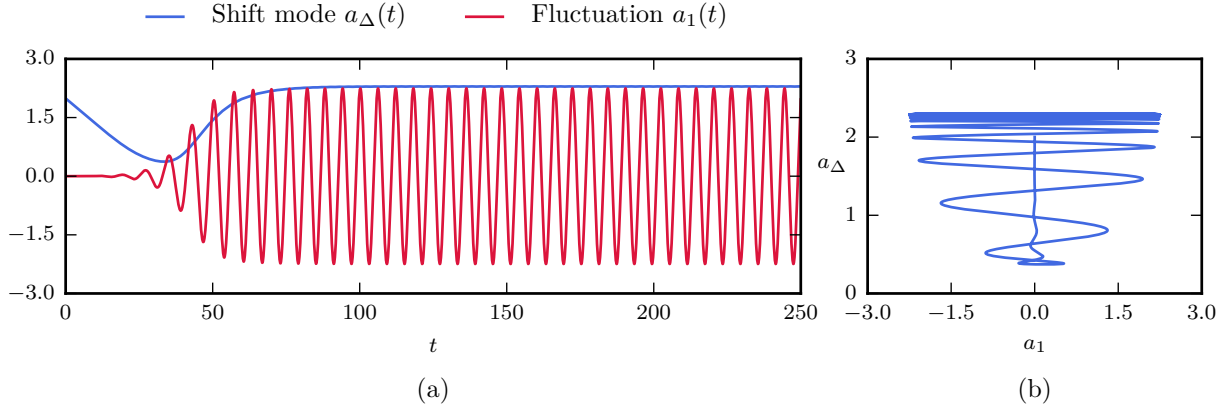


Figure 3: (a) Time evolution of the POD coefficients for the cylinder flow at $Re = 100$. The time evolution of $a_2(t)$, not shown, is very similar to that of $a_1(t)$. (b) Trajectory in the phase space projected onto the $a_1 - a_\Delta$ plane.

$$\frac{\partial \mathbf{u}}{\partial t} = -(\mathbf{U}_b \cdot \nabla) \mathbf{u} - (\mathbf{u} \cdot \nabla) \mathbf{U}_b - \nabla p + \frac{1}{Re} \nabla^2 \mathbf{u} - (\mathbf{u} \cdot \nabla) \mathbf{u} \quad (5)$$

$$\nabla \cdot \mathbf{u} = 0 \quad (6)$$

where \mathbf{U}_b is the base flow velocity field, \mathbf{u} is the perturbation velocity field and p the corresponding pressure. In order to ease the discussions to come, let us rewrite these equations as

$$\mathcal{B} \frac{\partial \mathbf{q}}{\partial t} = \mathcal{L} \mathbf{q} + \mathcal{N}(\mathbf{q}) \mathbf{q} \quad (7)$$

where $\mathbf{q} = (\mathbf{u}, p)^T$ is the perturbation state vector, \mathcal{L} is the linearised Navier-Stokes operator and $\mathcal{N}(\mathbf{q}) \mathbf{q} = -(\mathbf{u} \cdot \nabla) \mathbf{u}, 0)^T$ is the quadratic nonlinear term of equation (6). The matrix \mathcal{B} is a singular mass matrix defined such that $\mathcal{B} \mathbf{q} = \mathbf{u}$.

Despite its compact notation, equation (7) still is formally an infinite dimensional system, transformed into a very high-dimensional one once it is discretised. The aim of reduced-order modeling is thus to construct/derive/identify a system of the form

$$\frac{d\mathbf{a}}{dt} = \tilde{\mathcal{L}} \mathbf{a} + \tilde{\mathcal{N}}(\mathbf{a}) \mathbf{a} \quad (8)$$

where $\tilde{\mathcal{L}}$ and $\tilde{\mathcal{N}}(\mathbf{a}) \mathbf{a}$ are low-dimensional approximation of \mathcal{L} and $\mathcal{N}(\mathbf{q}) \mathbf{q}$, respectively, and where the entries of \mathbf{a} are the degrees of freedom of the reduced-order model. For the reduced-order model (8) to be a good approximation of its high-dimensional counterpart (7), the former needs to have the same properties as the latter. While this is implicitly true when the reduced-order model is derived based on a Galerkin projection and provided the projection basis includes the unstable eigenmodes, these properties might need to be enforced when a system identification approach as SINDy is used.

3.2.1 Constraining the linear term

As a starting point, let us consider the high- and low-dimensional linear terms \mathcal{L} and $\tilde{\mathcal{L}}$, respectively. Let us assume furthermore that a linear stability analysis of the high-dimensional system has been performed using *e.g.* a time-stepper approach (Bagheri et al., 2009; Edwards et al., 1994) such that the leading eigenvalues of \mathcal{L} are known *a priori*. In order for the reduced-order model (8) to be a faithful low-dimensional approximation of the original high-dimensional system (7) when infinitesimally small perturbations are considered, one needs

$$\text{eig}(\tilde{\mathcal{L}}) \subset \text{eig}(\mathcal{L})$$

i.e. the eigenvalues of the low-dimensional linear operator $\tilde{\mathcal{L}}$ form a subset of those of its high-dimensional counterpart \mathcal{L} . The constraint is thus

$$\det(\lambda \mathcal{I} - \tilde{\mathcal{L}}) = 0 \quad (9)$$

where \mathcal{I} is the identity matrix and λ is the known eigenvalue of the high-dimensional linear operator \mathcal{L} . Though this constraint and its gradient can be analytically derived for a 2×2 or 3×3 operator $\tilde{\mathcal{L}}$, $\det(\lambda \mathcal{I} - \tilde{\mathcal{L}})$ is a non-convex nonlinear function of the entries of $\tilde{\mathcal{L}}$. As a consequence, it cannot be handled by the CVXOPT library used in the present work and will not be discussed any further.

3.2.2 Constraining the quadratic nonlinear term

The nonlinear Navier-Stokes equations (6) are partial differential equations characterised by the quadratic nonlinear term $-(\mathbf{u} \cdot \nabla) \mathbf{u}$. In order to understand the role played by this quadratic nonlinear term, let us write down the Reynolds-Orr equation governing the evolution of the perturbation's kinetic energy

$$\frac{dE}{dt} = - \overbrace{\int_{\Omega} \mathbf{u} \cdot (\mathbf{u} \cdot \nabla) \mathbf{U}_b \, d\Omega}^{\text{Production}} - \underbrace{\frac{1}{Re} \int_{\Omega} \nabla \mathbf{u} : \nabla \mathbf{u} \, d\Omega}_{\text{Dissipation}} \quad (10)$$

where the boundary terms resulting from the integrations by parts are assumed to be small enough and can thus be neglected for the sake of simplicity. Though it can have a local influence, the transport term $-(\mathbf{U}_b \cdot \nabla) \mathbf{u}$ does not contribute to the total kinetic energy budget of the perturbation. Similarly, the contribution of the quadratic nonlinear term to the total energy of the perturbation is zero: it is an energy-preserving nonlinearity, its role being only to scatter the perturbation's energy along the different lengthscales of the problem.

Using the compact notation of (7), this energy-preserving property of the quadratic nonlinear term reads

$$\int_{\Omega} \mathbf{q} \cdot \mathcal{N}(\mathbf{q}) \mathbf{q} \, d\Omega = 0 \quad (11)$$

Given that our projection basis contains the POD modes, their amplitudes $a_i(t)$ is directly related to the kinetic energy of the perturbation. The constraint required in our system identification for the low-dimensional quadratic nonlinear term to be energy-preserving is thus

$$\mathbf{a} \cdot \tilde{\mathcal{N}}(\mathbf{a})\mathbf{a} = 0 \quad (12)$$

Hence, the matrix $\mathcal{N}(\mathbf{a})$ must also conserve energy, requiring it to be a skew-symmetric matrix

$$\mathcal{N}(\mathbf{a}) = \begin{bmatrix} 0 & \alpha a_1 + \beta a_2 + \gamma a_\Delta & \delta a_1 + \epsilon a_\Delta \\ -\alpha a_1 - \beta a_2 - \gamma a_\Delta & 0 & \zeta a_2 + \eta a_\Delta \\ -\delta a_1 - \epsilon a_\Delta & -\zeta a_2 - \eta a_\Delta & 0 \end{bmatrix} \quad (13)$$

Such a structure for the quadratic nonlinear term can be imposed by using a set of linear constraints on the regression coefficients.

3.2.3 What about higher order nonlinearities?

Reduced-order modelling based on Galerkin projection usually requires a relatively large projection basis. Despite the very low effective dimensionality of the cylinder flow at $Re = 100$, Noack et al. (2003) needed to include the first eight POD modes along with the shift mode for the reduced-order model to be a relatively faithful approximation of the original high-dimensional one. Though the perturbation velocity field can be correctly approximated using only the shift mode and the first two POD modes, including the higher harmonics POD modes was deemed necessary in order to avoid the energy overshoot otherwise observed during the nonlinear saturation process. It has been demonstrated that this overshoot and associated larger amplitude of the limit cycle and mean flow distortion are resulting from the disruption of the energy cascade induced by the truncation (Noack et al., 2003).

Even though the higher harmonics POD modes might be required to prevent a non-physical behaviour of the reduced-order model, they have very limited dynamics of their own: they are essentially *enslaved* to the dominant POD modes. Using *adiabatic elimination* (Haken, 1983) or *center manifold reduction* (Carini et al., 2015; Wiggins, 2003), it is well known that these slaved modes can be cast out of the problem, while their influence onto the driving ones be accounted for by modifying appropriately the nonlinearities, generally into higher-order ones. Such an approach to reduced-order modelling, which can be summarised as *derive-then-reduce*, has been used by ? to reduce the eight-dimensional system identified by Noack et al. (2003) into one having only three degrees of freedom, *i.e.* the amplitude of the shift mode and that of the first two POD modes.

Albeit doable, such derive-then-reduce approach is likely to involve cumbersome calculations, particularly if the original Galerkin projection model has more than just a few degrees of freedom. In the present work however, high-order nonlinearities modelling the influence of the truncated modes can be directly included in the identification process. For that purpose, the library $\Theta(\mathbf{a})$ of admissible functions needs to be extended in order to include higher-order polynomials. In the rest of this work, we will limit ourselves to a library $\Theta(\mathbf{a})$ made of all of the polynomials of \mathbf{a} up to the third degree. Note that it is relatively unclear at the present time what constraints should be included in the cost functional.

3.3 System identification

Two different libraries $\Theta(\mathbf{a})$ will be considered in the system identification problem: a library of quadratic polynomials and library of cubic polynomials, with 27 terms and 57 terms, respectively. Two different nonlinear reduced-order models have been identified. The first model, denoted model

A, has been identified using constraints enforcing the skew-symmetry of $\tilde{\mathcal{N}}(\mathbf{a})$, without cubic terms. The identified model is

$$\begin{bmatrix} \dot{a}_1 \\ \dot{a}_2 \\ \dot{a}_\Delta \end{bmatrix} = \left(\underbrace{\begin{bmatrix} 0.061 & -0.649 & 0 \\ -0.63 & 0.07 & 0 \\ 0 & 0 & -0.059 \end{bmatrix}}_{\tilde{\mathcal{L}}} + \underbrace{\begin{bmatrix} 0 & -0.176a_\Delta & -0.028a_1 \\ -0.176a_\Delta & 0 & -0.028a_2 \\ 0.028a_1 & 0.028a_2 & 0 \end{bmatrix}}_{\tilde{\mathcal{N}}(\mathbf{a})} \right) \begin{bmatrix} a_1 \\ a_2 \\ a_\Delta \end{bmatrix}. \quad (14)$$

The second reduced-order model, denoted model B, exhibits both quadratic and cubic nonlinearities. Once again, only the constraints enforcing the skew-symmetry of $\tilde{\mathcal{N}}(\mathbf{a})$ have been used. The identified model reads

$$\begin{bmatrix} \dot{a}_1 \\ \dot{a}_2 \\ \dot{a}_\Delta \end{bmatrix} = \left(\underbrace{\begin{bmatrix} 0.171 & -0.717 & 0 \\ 0.738 & 0.182 & 0 \\ 0 & 0 & -0.069 \end{bmatrix}}_{\mathcal{L}} + \underbrace{\begin{bmatrix} 0 & -0.143a_\Delta & -0.10a_1 \\ 0.143a_\Delta & 0 & -0.10a_2 \\ 0.10a_1 & 0.10a_2 & 0 \end{bmatrix}}_{\mathcal{N}(\mathbf{a})} + \underbrace{\begin{bmatrix} -0.012(a_1^2 + a_2^2) & 0.032(a_1^2 + a_2^2 - a_\Delta^2) & 0.023a_1a_\Delta \\ -0.031(a_1^2 + a_2^2 - a_\Delta^2) & -0.013(a_1^2 + a_2^2) & 0.025a_2a_\Delta \\ -0.04a_1a_\Delta & -0.04a_2a_\Delta & 0.011a_\Delta^2 \end{bmatrix}}_{\mathcal{C}(\mathbf{a}^2)} \right) \begin{bmatrix} x \\ y \\ z \end{bmatrix}. \quad (15)$$

Thanks to the sparsity promoting capabilities of our algorithm, this model has only twenty-one non-zero coefficients out of the fifty-seven possible. Moreover, the constrained regression identifies a system with the correct physical behaviour as will be shown in §4.

4 Discussion

Figure 4 provides a comparison of the dynamics predicted by the reduced-order models identified in the previous section. In all cases, the initial condition has an energy of 10^{-5} . From figure 4(a), it can be seen that the duration of transients is correctly predicted by model B while it is significantly over-estimated by model A. The difference between these two predictions relies in the spectral content of the linear operator $\tilde{\mathcal{L}}$ of each of the identified models. For model A, one has

$$\text{eig}(\tilde{\mathcal{L}}_A) = \begin{bmatrix} 0.065 + i0.64 & 0 & 0 \\ 0 & 0.065 - i0.64 & 0 \\ 0 & 0 & -0.059 \end{bmatrix} \quad (16)$$

while the eigenvalue decomposition of the linear operator in model B gives

$$\text{eig}(\tilde{\mathcal{L}}_B) = \begin{bmatrix} 0.177 + i0.73 & 0 & 0 \\ 0 & 0.177 - i0.73 & 0 \\ 0 & 0 & -0.07 \end{bmatrix} \quad (17)$$

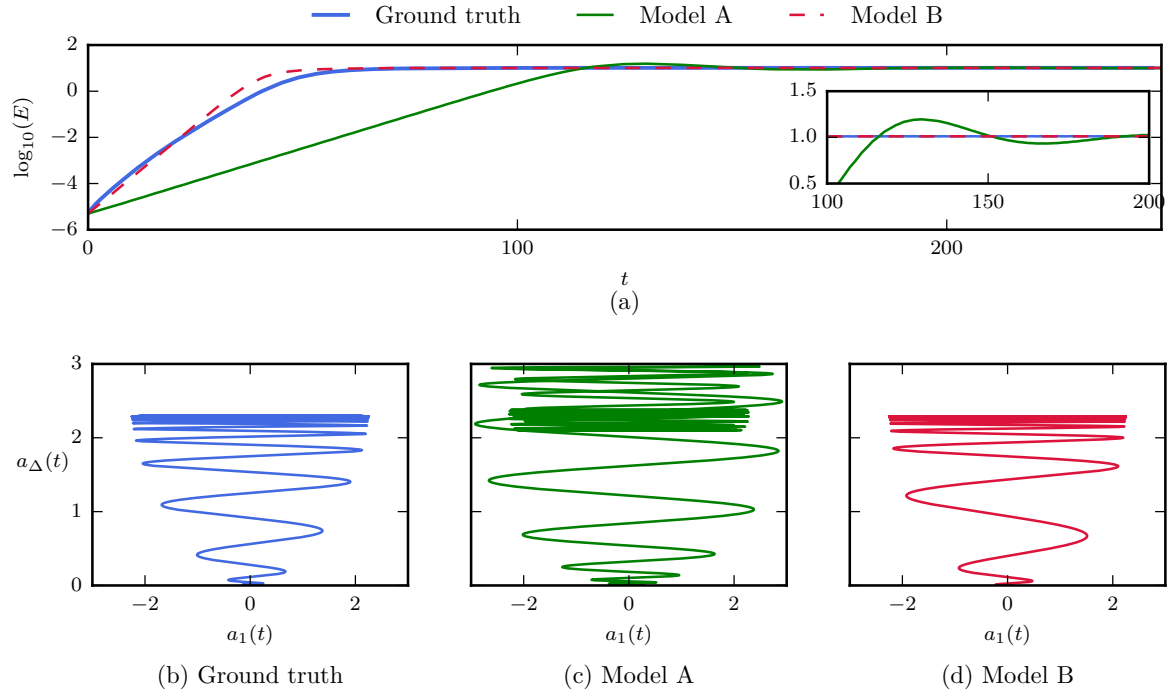


Figure 4: Comparison of the different reduced-order models identified. (a) Total energy $E = a_1^2 + a_2^2 + a_\Delta^2$ of the original and identified systems. The inset shows a close-up view of the nonlinear saturation process of model A in the range $100 \leq t \leq 150$. (b)–(d) Projection of the trajectory onto the (a_1, a_Δ) plane.

As shown, the growth rate of the fluctuation given by model A is almost three times smaller than that of model B, hence the longer duration of the transients. Similar over-estimation of the duration of the transients has been reported by Noack et al. (2003) when investigating Galerkin projection models using exclusively POD modes and the shift mode. Moreover, it must be noted that the quadratic model suffers from an energy overshoot when nonlinear saturation occurs. During this saturation process, the amplitude of the mean flow distortion $z(t)$ is over-estimated by almost 50%. It also over-estimates the amplitude of the final limit cycle by almost 3% and the saturation of the mean flow distortion by 1%. As discussed by Noack et al. (2003), this energy overshoot, the larger amplitude of the limit cycle and the slightly higher saturation of the mean flow distortion are all related to the interruption of the energy-flow cascade due to higher harmonic POD modes being neglected in the quadratic model. Being absent from the model, the higher harmonics cannot absorb the excess energy produced by the two most energetic modes. The latter then grow beyond the correct value until the mean-flow distortion $a_\Delta(t)$ can eventually absorb this excess energy via the coupling terms in (14).

The time evolution of the energy predicted by model B with cubic nonlinearities is also depicted in figure 4(a) while the trajectory projected onto the $a_1 - a_\Delta$ plane is shown in figure 4(c). From these figures, it can be seen that the dynamics of the original system and the ones predicted by model B are almost identical. The amplitude of the limit cycle predicted by model B is only 0.5% higher than that of the original system while the saturation of the mean flow distortion differs by less than 0.1%. The excellent prediction of model B as well as the parallels drawn with amplitude equations (Noack and Eckelmann, 1994; Sipp and Lebedev, 2007), adiabatic elimination (Haken, 1983) or center manifold reduction (Carini et al., 2015; Wiggins, 2003) thus justify *a posteriori* the use of higher-order nonlinearities in the system identification to model the influence of the truncated modes onto the driving ones. It is also interesting to note that including higher-order nonlinearities in the identification library appears to cure the behaviour of the linear operator of the reduced-order model as shown in the eigenvalue decomposition of $\tilde{\mathcal{L}}$.

Finally, plotting the trajectories given by the different models has proven helpful in order to draw connections with the reduced-order models obtained by Noack et al. (2003) based on a Galerkin projection procedure. By comparing figure 4(a) and (b) of the present paper against figures 11, 13, 15 and 16 of Noack et al. (2003), it appears that Model A shares close connections with the standard *Galerkin models* of Noack et al. (2003) where the eight most energetic modes and the shift mode have been considered in the Galerkin projection. A proper comparison against such models obtained by Galerkin projection is currently under investigation.

5 Conclusion

This paper generalizes the sparse identification of nonlinear dynamics (SINDy) algorithm (Brunton et al., 2016) to include additional constraints required to guarantee energy conservation or satisfy other inherent symmetries. These constraints may be pre-defined and enforced directly in the sparsity-promoting regression. The emblematic two-dimensional cylinder flow at $Re = 100$ has been used to illustrate the system identification capabilities of the resulting algorithm. For that purpose, two polynomial libraries have been used and the constraints have been chosen in order to enforce different physical properties. Both identified models qualitatively reproduce the main features of the original system: linear instability of the fixed point and final saturation to a periodic

limit cycle. Though these models rely essentially on a data-driven approach, visual inspection of their trajectories in the phase space highlights possible connections between the quadratic model A and the models obtained using a Galerkin projection procedure in the seminal work of Noack et al. (2003).

Comparing the quadratic and cubic reduced-order models, it appears that the overall predictive capabilities and quality of the identified models depend on the library $\Theta(\mathbf{a})$ and constraints used in the identification phase. To our knowledge, the second model presented herein (model B) is among the simplest and yet most efficient reduced-order models available in the literature to simulate both the transients and nonlinearly saturated dynamics of the cylinder flow at $Re = 100$. This model includes cubic nonlinearities to take into account the influence of truncated modes, something which can be justified by drawing a parallel with adiabatic elimination and center manifold reduction (Carini et al., 2015; Haken, 1983; Wiggins, 2003). Though such result is very promising, it has to be noted that it is not yet clear how successful such a model identification strategy would be when applied to a system characterised by a large number of degrees of freedom.

References

- M. S. Andersen, J. Dahl, and L. Vandenberghe. CVXOPT: A Python package for convex optimization, Version 1.1.6, 2013.
- S. Bagheri. Koopman-mode decomposition of the cylinder wake. *J. Fluid Mech.*, 726:596–623, 2013.
- Shervin Bagheri, Espen Åkervik, Luca Brandt, and Dan S Henningson. Matrix-free methods for the stability and control of boundary layers. *AIAA journal*, 47(5):1057–1068, 2009.
- M. J. Balajewicz, E. H. Dowell, and B. R. Noack. Low-dimensional modelling of high-Reynolds-number shear flows incorporating constraints from the Navier–Stokes equation. *J. Fluid Mech.*, 729:285–308, 2013.
- D. Barkley and R. D. Henderson. Three-dimensional Floquet stability analysis of the wake of a circular cylinder. *J. Fluid Mech.*, 322:215–241, 1996.
- G. Berkooz, P. J. Holmes, and J. L. Lumley. The proper orthogonal decomposition in the analysis of turbulent flows. *Annual review of fluid mechanics*, 25(1):539–575, 1993.
- J. Bongard and H. Lipson. Automated reverse engineering of nonlinear dynamical systems. *Proceedings of the National Academy of Sciences*, 104(24):9943–9948, 2007.
- S. L. Brunton and B. R. Noack. Closed-loop turbulence control: Progress and challenges. *Applied Mechanics Reviews*, 67(5):050801, 2015.
- S. L. Brunton, J. L. Proctor, and J. N. Kutz. Discovering governing equations from data by sparse identification of nonlinear dynamical systems. *Proceedings of the National Academy of Sciences*, 113(15):3932–3937, 2016.
- M. Carini, F. Auteri, and F. Giannetti. Centre-manifold reduction of bifurcating flows. *J. Fluid Mech.*, 767:109–145, 3 2015. ISSN 1469-7645. doi: 10.1017/jfm.2015.3. URL http://journals.cambridge.org/article_S0022112015000038.

- N. R. Draper and H. Smith. *Applied regression analysis*. John Wiley & Sons, 2014.
- WS Edwards, Laurette S Tuckerman, Richard A Friesner, and DC Sorensen. Krylov methods for the incompressible navier-stokes equations. *Journal of computational physics*, 110(1):82–102, 1994.
- N. Fabbiane, O. Semeraro, S. Bagheri, and D. S. Henningson. Adaptive and model-based control theory applied to convectively unstable flows. *Applied Mechanics Reviews*, 66(6):060801, 2014.
- P.F. Fischer, J.W. Lottes, and S.G. Kerkemeir. Nek5000 Web pages, 2008. <http://nek5000.mcs.anl.gov>.
- G. H. Golub and C. F. Van Loan. *Matrix computations*, volume 3. JHU Press, 2012.
- H Haken. Springer series in synergetics. *Editors: M. Cardona P. Fulde H.-J. Queisser*, page 269, 1983.
- P. J. Holmes, J. L. Lumley, G. Berkooz, and C. W. Rowley. *Turbulence, coherent structures, dynamical systems and symmetry*. Cambridge Monographs in Mechanics. Cambridge University Press, Cambridge, England, 2nd edition, 2012.
- E. Jones, T. Oliphant, P. Peterson, et al. SciPy: Open source scientific tools for Python, 2001. URL <http://www.scipy.org/>. [Online; accessed 2016-07-06].
- A. J. Majda and J. Harlim. Physics constrained nonlinear regression models for time series. *Non-linearity*, 26(1):201, 2012.
- B. R. Noack and H. Eckelmann. A global stability analysis of the steady and periodic cylinder wake. *J. Fluid Mech.*, 270:297–330, 1994.
- B. R. Noack, K. Afanasiev, M. Morzynski, G. Tadmor, and F. Thiele. A hierarchy of low-dimensional models for the transient and post-transient cylinder wake. *J. Fluid Mech.*, 497:335–363, 2003.
- B. R. Noack, W. Stankiewicz, M. Morzynski, and P. J. Schmid. Recursive dynamic mode decomposition of a transient cylinder wake. *arXiv preprint arXiv:1511.06876*, 2015.
- M. Schmidt and H. Lipson. Distilling free-form natural laws from experimental data. *science*, 324(5923):81–85, 2009.
- M. Schumm, B. Eberhard, and P. A. Monkewitz. Self-excited oscillations in the wake of two-dimensional bluff bodies and their control. *J. Fluid Mech.*, 271:17–53, 1994.
- R. Semaan, P. Kumar, M. Burnazzi, G. Tissot, L. Cordier, and B. R. Noack. Reduced-order modelling of the flow around a high-lift configuration with unsteady coanda blowing. *Journal of Fluid Mechanics*, 800:72–110, 8 2016. ISSN 1469-7645. doi: 10.1017/jfm.2016.380. URL http://journals.cambridge.org/article_S0022112016003803.
- T. K. Sengupta, S. I. Haider, M. K. Parvathi, and G. Pallavi. Enstrophy-based proper orthogonal decomposition for reduced-order modeling of flow past a cylinder. *Physical Review E*, 91(4):043303, 2015.

- D. Sipp and A. Lebedev. Global stability of base and mean flows: a general approach and its applications to cylinder and open cavity flows. *J. Fluid Mech.*, 593:333–358, 2007.
- D. Sipp and P. J. Schmid. Linear closed-loop control of fluid instabilities and noise-induced perturbations: A review of approaches and tools. *Applied Mechanics Reviews*, 68(2):020801, 2016.
- L. Sirovich. Turbulence and the dynamics of coherent structures. Part I: Coherent structures. *Quarterly of Applied Mathematics*, 45(3):561–571, 1987.
- G. Tadmor, O. Lehmann, B. R. Noack, and M. Morzyński. Mean field representation of the natural and actuated cylinder wake. *Physics of Fluids (1994-present)*, 22(3):034102, 2010.
- S. Wiggins. *Introduction to applied nonlinear dynamical systems and chaos*, volume 2 of *Texts in Applied Mathematics*. Springer Science & Business Media, Berlin, Heidelberg, 2003.
- A Zebib. Stability of viscous flow past a circular cylinder. *Journal of Engineering Mathematics*, 21(2):155–165, 1987.
- H.-Q. Zhang, U. Fey, B. R. Noack, M. König, and H. Eckelmann. On the transition of the cylinder wake. *Physics of Fluids (1994-present)*, 7(4):779–794, 1995.